Shear-Induced Lamellar Rotation Observed in a Diblock Copolymer by in Situ Small-Angle X-ray Scattering

ARTICLE *in* MACROMOLECULES · JUNE 1999

Impact Factor: 5.8 · DOI: 10.1021/ma981796d

6 AUTHORS, INCLUDING:

Steven D. Smith
Procter & Gamble
109 PUBLICATIONS **3,207** CITATIONS
SEE PROFILE

Nicholas J Terrill
Diamond Light Source
93 PUBLICATIONS **1,714** CITATIONS
SEE PROFILE

David C Morse
University of Minnesota Twin Cities
79 PUBLICATIONS **2,158** CITATIONS
SEE PROFILE

Karen I Winey
University of Pennsylvania
331 PUBLICATIONS **11,308** CITATIONS
SEE PROFILE

Shear-Induced Lamellar Rotation Observed in a Diblock Copolymer by in Situ Small-Angle X-ray Scattering

D. L. Polis,[†] S. D. Smith,[‡] N. J. Terrill,[§] A. J. Ryan,[||] D. C. Morse,[⊥] and K. I. Winey*[,†]

Laboratory for Research on the Structure of Matter, Department of Materials Science and Engineering, University of Pennsylvania, Philadelphia, Pennsylvania 19104-6272, Corporate Research Division, The Procter and Gamble Company, Cincinnati, Ohio 45239-8707, CLRC, Daresbury Laboratory, Warrington, WA4 4AD United Kingdom, Department of Chemistry, University of Sheffield, Sheffield, S3 7HF United Kingdom, and Department of Chemical Engineering and Materials Science, University of Minnesota, Minneapolis, Minnesota 55455-0132

Received November 18, 1998

ABSTRACT: In situ small-angle X-ray scattering (SAXS) rheology is used to study the dynamic process of shear alignment in a lamellar poly(styrene-*b*-ethylene propylene) diblock copolymer, at temperatures far below the microphase separation transition temperature. We have focused on the alignment dynamics at time scales shorter than 1 cycle of deformation. To extract this valuable information, we use prealigned specimens and follow subtle changes in the orientation during a steady shear deformation. Two notable changes in the azimuthal SAXS intensity are observed: the maximum of the main peak induced during prealignment shifts to lower azimuthal angles and a secondary peak develops and shifts to higher angles. We effectively modeled the shift of the main peak maximum by assuming that lamellae rotate with the vorticity component of shear. This provides conclusive evidence for lamellar rotation in block copolymers, as opposed to a discontinuous transformation such as lamellar dissolution and reformation. Lamellar rotation also supports our previously proposed mechanism for kink band formation.

Introduction

Understanding the mechanisms of shear-induced alignment in lamellar block copolymers is of fundamental and practical importance. Because lamellar block copolymers have longer relaxation times than their small molecule smectic counterparts, they serve as model systems for studying the response of layered viscoelastic fluids subjected to shear fields. From a practical standpoint, understanding the mechanisms and kinetics of shear alignment provides a framework for guiding processing and thus controlling the macroscopic orientations induced by shear. Specifically, this knowledge can be used to avoid various defect structures, such as conjugate kink bands,[1] thereby optimizing uniaxial orientations. Furthermore, a clear understanding of alignment mechanisms would enable the exploitation of various nonequilibrium or transient shear-induced morphologies.

Much experimental work has been devoted to characterizing the final state of alignment in lamellar block copolymers as a function of molecular architecture and processing conditions.[2,3] To date, uniaxial parallel and uniaxial perpendicular orientations have been induced in the bulk by large amplitude oscillatory shear (LAOS) in both poly(styrene-*b*-isoprene) (PS−PI) type[4−16] and poly(ethylene propylene-*b*-ethylethylene) (PEP−PEE) type[17−19] lamellar diblock systems. Additionally, LAOS has been used to induce mixed bulk morphologies, composed primarily of parallel and perpendicular orientations in a PS−PI system[20] and parallel−transverse biaxial orientations in PS−PI and PS−PEP systems.[1,6,9,21,22] To complicate matters, in situ rheo-optical experiments have revealed that there are multiple pathways leading to a parallel orientation: one that passes through a parallel−perpendicular transient orientation and one that passes through a parallel−transverse transient orientation.[7,11,13,14] These pathways, leading to distinct transient lamellar distributions, were observed near the microphase separation transition temperature, T_{MST}, in low-molecular-weight systems. Parallel−transverse morphologies have also been produced far from T_{MST}, in higher molecular-weight systems. In contrast to low-molecular-weight systems near T_{MST}, these parallel−transverse morphologies appear to reach a steady state during oscillatory shear.[6,21] The fact that multiple orientations, both uniaxial and biaxial, and multiple pathways can be induced by LAOS in a single chemical system clearly suggests that a variety of mechanisms compete during shear-induced alignment. These mechanisms may act independently or in conjunction with each other to varying degrees, depending on things such as the time scale of the deformation relative to the characteristic relaxation times of the material, the extent of mechanical contrast between alternating lamellae, the degree of phase separation, and the effect of defects. An understanding of these alignment mechanisms is essential if one hopes to push the limits of morphological control, e.g., from currently available uniaxial orientation distributions to true single-crystal-type morphologies. This leap in understanding/control would make these self-assembled materials considerably more attractive in the growing number of applications that require structural elements at the nanometer scale.

While many mechanisms have been proposed, such as lamellar dissolution/reformation, grain rotation, and defect migration, there are experimental barriers to clearly identifying them.[3] Electron microscopy provides a picture of the lamellar structure, and if one could

* To whom correspondence should be addressed.
[†] University of Pennsylvania.
[‡] The Procter and Gamble Company.
[§] Daresbury Laboratory.
[||] University of Sheffield.
[⊥] University of Minnesota.

10.1021/ma981796d CCC: $18.00
Published on Web 06/16/1999

follow the deformation process with in situ microscopy, an understanding of shear alignment would be straightforward. While this type of in situ microscopy is not currently possible, we have shown that by focusing on a particular morphological feature, one can gain insight about dynamic information from ex situ microscopy. Specifically, we have identified kink bands as the defect structure responsible for the previously observed parallel−transverse biaxial orientations induced far below T_{MST}. Rather than following the alignment procedure over 10s to 1000s of cycles, we started with a nearly aligned morphology and induced kink bands with steady shear. The strain dependence of the kink band morphology is consistent with a fixed hinge model, suggesting that kink bands initiate at defects and grow by lamellar rotation.[1]

The current in situ small-angle X-ray scattering (SAXS) rheology experiments were designed to demonstrate the role of defects in kink band initiation and verify the growth mechanism for kink bands. As opposed to other in situ SAXS rheology experiments, where a great deal of information is lost due to summing the scattered intensities during forward−reverse shearing, we examine unidirectional or steady shear. In a further attempt to simplify the problem, we start with a prealigned specimen, similar to the approach of Scott et al.,[23] rather than an isotropic distribution of lamellar domains. To maximize strain resolution, synchrotron radiation and very slow shear rates were used, such that scattering patterns were obtained every 0.15 strain units. Furthermore, in one sample silica spheres were dispersed in the lamellar diblock copolymer in an attempt to increase the volume fraction of kink bands, thus increasing the scattered intensity from these structures. By starting with a well-aligned starting state, simplifying the strain profile, and maximizing strain resolution, we are able to follow subtle changes in the lamellar orientation with time (strain). Comparing the scattered intensities from the block copolymer with and without silica spheres allows us to separate the contributions due to kink bands.

Two important changes in the azimuthal intensity are observed as a function of strain. These changes in the azimuthal intensity were modeled using the scattering profile of the starting state and a dynamic equation describing the response of lamellae under shear. This approach captures the salient features of the scattered intensities as a function of strain, enabling us to extract dynamic information about lamellae in the matrix and in the kink bands. This work provides conclusive evidence for shear-induced lamellar rotation. Furthermore, we demonstrate that the volume fraction of kink band defects can be systematically controlled through the addition of silica spheres. Both results provide additional control over the shear-induced nanopatterns in block copolymers.

Experimental Section

Material. The lamellar poly(styrene-*b*-ethylene propylene) diblock copolymer studied was prepared by selective hydrogenation of a PS−PI diblock copolymer synthesized by living anionic polymerization.[24] The polystyrene (PS) block has a weight-average molecular weight, M_w, of 38 000 and the diblock copolymer has a polydispersity index of 1.02. The molecular weight and polydispersity index were determined by size exclusion chromatography, with Ultrastyragel columns of 500, 1000, 10 000, and 100 000 Å porosity, in tetrahydrofuran relative to PS standards. The diblock copolymer is 38 wt % PS, as determined by ^{1}H NMR analysis using a GE QE-300 NMR. It will therefore be referred to as SEP(38−62), corresponding to the nominal M_w's of the PS and poly(ethylene propylene) (PEP) blocks.

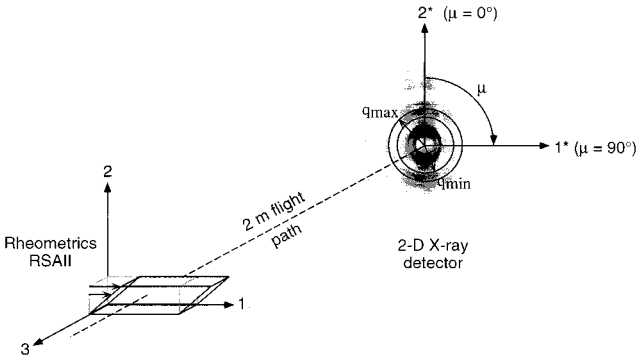

Figure 1. Schematic showing the geometry of the in situ SAXS rheology experiment. An RSAII was used to prealign the specimens and apply the steady shear deformations. The 1, 2, and 3 directions correspond to the velocity, velocity-gradient, and neutral directions, respectively. The X-ray beam was oriented along the 3 direction, to follow azimuthal scattering intensity in the 1*−2* scattering plane. An area detector was located 2 m from the sample. Azimuthal scans were obtained by integrating about the fourth-order Bragg peak (q_{min} to q_{max}), to give scattered intensity as a function of azimuthal angle, μ. Parallel and transverse lamellae scatter along the 2* (μ = 0°, ±180°) and 1* (μ = ±90°) directions, respectively. Note, the schematic illustrates "positive" steady shear in the experimental reference frame. Schematic is rotated relative to laboratory coordinates; shearing direction is vertical.

Two samples were prepared by solvent casting in toluene. The solutions (∼6 wt %) of SEP(38−62) with less than 1 wt % antioxidant (Irgonox 1010 from Ciba-Geigy) were dried in Teflon pans such that the dried films had a final thickness of ∼1 mm. In one of the samples, 0.5 vol % silica spheres, coated with $CH_3(CH_2)_{16}CH_3$, were added to the solution after they had been sonicated in toluene for 1 h. The coated silica spheres (Monospher 500C from Merck and Company, Inc.) have a diameter of 0.5 μm. In both samples the solvent was slowly evaporated in air, at room temperature, for 6 days. The samples were then dried under vacuum for 24 h at 30 °C, followed by 24 h at 120 °C, and finally 48 h at 150 °C. The samples were compression-molded to a final thickness of 0.5 mm for shearing studies. We will refer to the samples as SEP(38−62)O and SEP(38−62)X, corresponding to the lamellar diblock sample with and without silica spheres.

SAXS Rheology. Steady shear experiments with in situ SAXS were performed on beam line 16.1 at Daresbury Laboratory, Warrington, U.K. Figure 1 illustrates the experimental geometry. A Rheometrics solids analyzer (RSAII), with shear sandwich geometry, was used to prealign the specimens with oscillatory shear and to apply the steady shear deformations. Specially constructed "match-stick" tools were used such that the shearing geometry was rotated 90°, relative to the standard RSAII configuration, to allow for in situ scattering along the neutral direction. The sample dimensions were 12 × 0.5 × 4 mm^3 along the velocity (1), velocity-gradient (2), and neutral (3) directions, respectively. An area detector, with 512 × 512 resolution, was located 2 m from the sample. Details regarding monochromation, collimation, detection, and wavelength of the X-rays at beam line 16.1 can be found elsewhere.[25]

Large amplitude oscillatory shear (LAOS) was used to prealign the specimens in a predominately parallel orientation (lamellar normal parallel to the 2 direction). In our previous work we demonstrated that strain ramping was effective in aligning a similar SEP diblock copolymer, thus avoiding a parallel−transverse biaxial orientation.[1] Therefore, the fol-

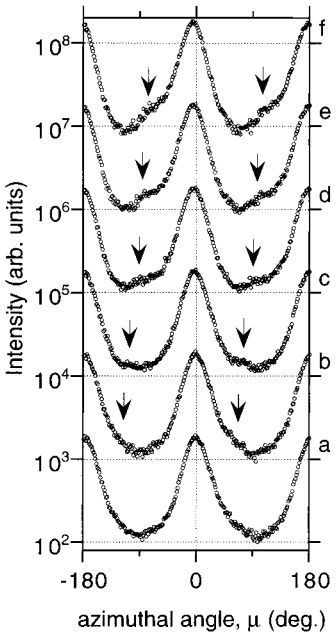

Figure 2. Azimuthal scattered intensity acquired in situ for SEP(38−62)X following (a) the prealignment procedure and during steady shear (180 °C, 0.005 s^{-1}): (b) 0 to 15%, (c) 15 to 30%, (d) 30 to 45%, (e) 45 to 60%, and (f) 60 to 75% strain. The azimuthal profiles were shifted by factors of 10 for clarity.

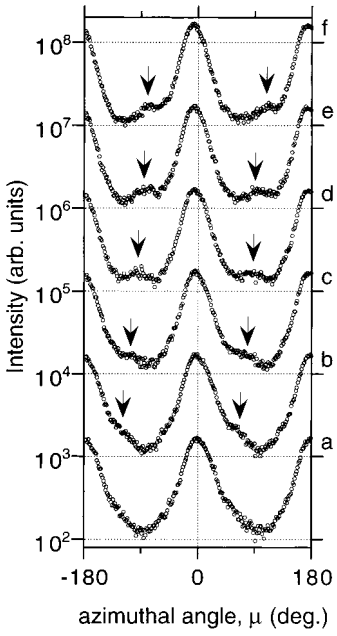

Figure 3. Azimuthal scattered intensity acquired in situ for SEP(38−62)O following (a) the prealignment procedure and during steady shear (180 °C, 0.005 s^{-1}): (b) 0 to 15%, (c) 15 to 30%, (d) 30 to 45%, (e) 45 to 60%, and (f) 60 to 75% strain. The azimuthal profiles were shifted by factors of 10 for clarity.

lowing strain-ramping procedure was used: 15 min of LAOS ($\gamma_0 = 20\%$) followed by 45 min of LAOS ($\gamma_0 = 40\%$), both at a frequency of 1 rad/s and 180 °C. Quiescent annealing in the rheometer at 180 °C for 66 min followed strain ramping. After the prealignment, specimens were sheared at a constant rate of 0.005 s^{-1} to a strain of 80% followed by shearing in the opposite direction (shear rate = −0.005 s^{-1}) to −80%.

A 36-s SAXS pattern was collected at the end of the 66-min annealing period, which serves as our reference for the steady shear experiments, and will be referred to as the "starting state". During the steady shear deformation, SAXS patterns were collected for 3 s with 10-μs intervals between collections. An ion chamber, located before the sample, was used to correct for changes in the beam current with time. Ten 3-s frames were added, producing SAXS patterns that correspond to a 30-s collection time or a 15% strain increment. This strain resolution is possible because of the very slow strain rates and high-intensity synchrotron radiation. Azimuthal scans were obtained, for both the starting state and steady shear patterns, by integrating about the fourth-order Bragg peak. This peak was chosen because the third-order peak is absent due to a minimum in the form factor, and the second-order peak was partially obscured by the beam stop.

Results

The starting state SAXS patterns, obtained prior to steady shear, for SEP(38−62)X and SEP(38−62)O are shown in Figure 2a and 3a, respectively. Scattering maximum at 0° and ±180° indicate a parallel orientation for both samples. However, it is important to note that the azimuthal intensity is not a δ function but rather a unimodal intensity distribution centered at 0° (fwhm = 35° and 41° for SEP(38−62)X and SEP(38−62)O, respectively), corresponding to a distribution of lamellar orientations. From our previous electron microscopy study, we found that residual defects in the starting state can cause neighboring lamellae to change orientation in a particular way, forming S-folds, which appear to be precursors to kink bands.[1] These S-folds, as well as other nonparallel lamellae, lead to a distribution of lamellar orientations.

Figure 2 shows the azimuthal intensity for SEP(38−62)X as a function of strain, during the forward (positive) steady shear deformation. Each azimuthal scan, with the exception of (a) the starting state data, represents SAXS data collected in situ over a 15% strain increment: (b) 0 to 15%, (c) 15 to 30%, (d) 30 to 45%, (e) 45 to 60%, and (f) 60 to 75%. The data in this and subsequent figures that show the strain dependence of the scattering intensity have been shifted vertically, by a factor of 10 between successive values of strain. The relation between the direction of positive shear and the azimuthal scattering angle μ is shown in Figure 1; the vorticity of the flow during positive shear is to tend to rotate lamellar domains to higher values of μ. Two important changes in the scattering intensity $I(\mu,t)$ are observed with increasing strain or time. (i) The position of the maximum in the main peak rotates from its initial position $\mu = 0°$ to values $\mu < 0°$, as if it were rotating in the direction opposite the vorticity of the flow. (ii) The right shoulder ($\mu > 0°$) of the main peak develops into a secondary peak, which shifts to higher angles with increasing strain, as shown by the arrows. Figure 3 shows the equivalent sequence of azimuthal scans for SEP(38−62)O, which is the sample with silica spheres. The same two features are evident, but the development and shift of the secondary peak (indicated by the arrows) is more pronounced in this sample.

Figure 4 shows the azimuthal intensity for SEP(38−62)O as a function of strain, during the first half of the reverse (negative) steady shear deformation, 75 to 0% strain, collected in 15% strain increments. With the shearing direction reversed, the maximum of the main peak shifts to larger angles, returning to $\mu = 0°$ at 0% strain. Similarly, a change in the direction of peak rotation is observed for the secondary peak, which shifts to lower angles and rejoins the main peak, essentially

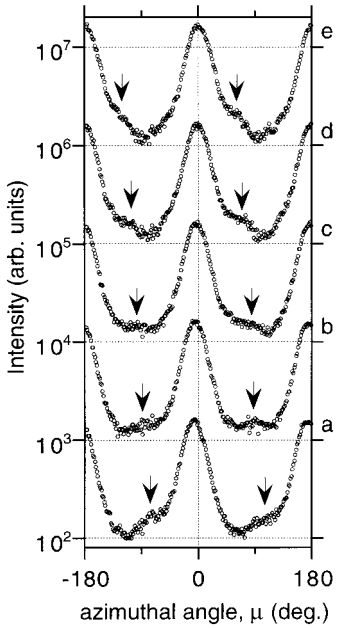

Figure 4. Azimuthal scattered intensity acquired in situ for SEP(38−62)O during steady shear in the reverse direction (180 °C, −0.005 s^{-1}) relative to the deformation shown in Figure 3. (a) 75 to 60%, (b) 60 to 45%, (c) 45 to 30%, (d) 30 to 15%, and (e) 15 to 0% strain. The azimuthal profiles were shifted by factors of 10 for clarity.

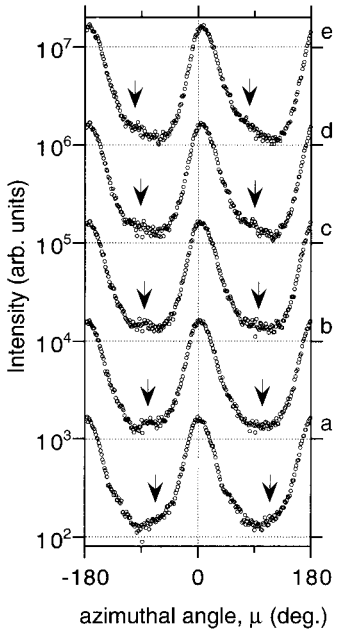

Figure 5. Azimuthal scattered intensity acquired in situ for SEP(38−62)O during steady shear in the same direction as the deformation described in Figure 4. (a) 0 to −15%, (b) −15 to −30%, (c) −30 to −45%, (d) −45 to −60%, and (e) −60 to −75% strain. The azimuthal profiles were shifted by factors of 10 for clarity.

following a trajectory reverse to that shown in Figure 3. Figure 5 shows the azimuthal intensity for SEP(38−62)O as a function of strain, during the second half of the negative steady shear deformation, 0 to −75% strain. The maximum of the main peak continues to shift to larger angles. A "new" secondary peak develops to the left of the main peak and shifts to lower angles. In summary, from 75 to −75% strain the maximum of the main peak shifts to higher angles, passing through $\mu = 0°$ at 0% strain, while two smaller peaks shift to lower angles, both passing through the transverse orientation ($\mu = \pm 90°$).

Analysis

Our goal in this section is to describe and partly explain the evolution of the observed scattering intensity during an imposed forward steady shear.

We assume that the intensity $I(\mu,t)$ is proportional to the volume fraction of lamellar domains with unit normals that lie within the 1−2 plane and are misaligned from the 2 axis by an azimuthal angle μ at time t (see Figure 1 for the coordinate system). In our previous electron microscopy study of kink bands,[1] we obtained results that suggested that the lamellae within kink bands rotate during shear flow, while each kink band maintains a nearly constant width. If we assume that the distribution of orientations evolves purely by rotation around the vorticity (3) axis, and that domain normals that lie within the 1−2 plane thus remain within this plane under rotation, then we may interpret $I(\mu,t)$ as a conserved probability density that obeys a differential conservation law[26] of the form

$$\frac{\partial I(\mu,t)}{\partial t} = -\frac{\partial}{\partial \mu}(\dot{\mu}(\mu,t) I(\mu,t)) \tag{1}$$

in which $\dot{\mu}(\mu,t)$ is the rate of rotation of domains with orientation μ at time t. The effects of boundary migration would generally not be describable by a differential equation of this form. In boundary migration, one lamellar orientation grows at the expense of another with a significantly different orientation by motion of a tilt boundary between them, leading to a direct transfer of intensity between widely separated values of μ. In general, a differential conservation law cannot describe mechanisms that produce a discontinuous change in orientation, such as boundary migration or dissolution/reformation.

To construct a simple phenomenological model for the rate of rotation at a fixed shear rate, we assume the following. (i) The rate of rotation may be approximated by a function $\dot{\mu} = \dot{\mu}(\mu)$ dependent on μ alone. Any such function must be periodic in μ with a period π, since orientations μ and $\mu + n\pi$ are physically equivalent for integer n. (ii) The rate of rotation vanishes for the aligned orientation $\mu = 0$ (and equivalent values of $\mu = n\pi$). (iii) The rate of rotation is positive (clockwise) for all other values of μ during positive shear. The simplest algebraic relation that satisfies these assumptions, to which we will compare the data, is

$$\dot{\mu} = k \sin^2(\mu) \tag{2}$$

where k is the effective strain rate. If k is set equal to the actual strain rate, then eq 2 becomes equivalent to the expression for the rate of rotation of a thin rigid rod in a two-dimensional shear flow.

To solve eq 1, it is useful to introduce a function

$$F(\mu,t) = \int_{-\pi}^{\mu} I(\mu,t)\, \mathrm{d}\mu \tag{3}$$

such that $\partial F/\partial \mu = I$. We use the fact that if lamellae rotate according to some deterministic rule (e.g., eq 2) such that the orientation $\mu(t)$ of a lamellar domain at

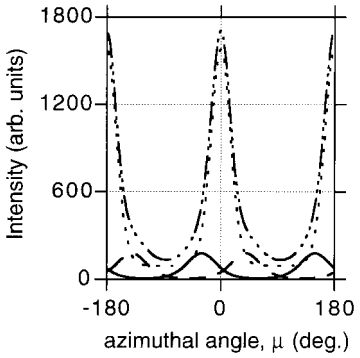

Figure 6. Plot showing the three modified Gaussian peaks used to fit the starting state data, $I(\mu,0)$, of SEP(38−62)O. The form of these Gaussian peaks is described by eq 9. Because the scattering patterns are periodic with respect to μ, $\sin^2(\mu - \mu_0)$ terms are used in the exponential, producing peaks centered at μ_0 and $\mu_0 \pm 180°$ for each of the three Gaussian peaks. These peaks will be referred to as left, middle, and right, corresponding to their peak centers relative to $\mu = 0°$. The left (solid line) and right (dashed line) Gaussian peaks are nearly symmetrical with respect to the middle (dotted line) Gaussian. The middle Gaussian contains a baseline term, which accounts for the isotropic scattering from randomly oriented lamellar grains, whereas the left and right Gaussian peaks decay to zero intensity. The fit to the starting state (dot−dashed line) is the sum of the left, middle, and right Gaussian peaks.

time t can be obtained given its orientation $\mu(0)$ at time $t = 0$ by a mapping

$$\mu(t) = f(\mu(0),t) \tag{4}$$

for which we may define a corresponding inverse mapping

$$\mu(0) = g(\mu(t),t) \tag{5}$$

then

$$F(\mu,t) = F(g(\mu,t),0) \tag{6}$$

The corresponding prediction for the X-ray scattering at time t is given by the partial derivative

$$I(\mu,t) = \frac{\partial F(\mu,t)}{\partial \mu} = \frac{\partial g(\mu,t)}{\partial \mu}\frac{\partial F(\mu',0)}{\partial \mu'}\Big|_{\mu'=g(\mu,t)} \tag{7}$$

Integrating eq 2 yields $kt = \cot(\mu(0)) - \cot(\mu(t))$, which may be solved for $\mu(0)$ to give an inverse mapping

$$g(\mu,t) = \cot^{-1}[kt + \cot(\mu)] \tag{8}$$

We now apply this model to the scattering data obtained during positive steady shear of SEP(38−62)X and SEP(38−62)O. The scattering distributions $I(\mu,0)$ of the starting states, Figures 2a and 3a, have been accurately fit by a sum of three functions, each of which is a modified Gaussian plus a constant offset,

$$I(\mu,0) = \sum_{i=1}^{3}\{y_{0i} + \lambda_i \exp[-\beta_i \sin^2(\mu - \mu_{0i})]\} \tag{9}$$

where the modified Gaussian contributions have been written as exponentials of $\sin^2(\mu - \mu_{0i})$ to guarantee that the function is periodic in μ with a period π. Figure 6 shows the three curves used to fit the starting state data for SEP(38−62)O. The middle Gaussian is much larger than the other two and is centered at $\mu = 0$, while the smaller left and right Gaussian peaks are displaced nearly symmetrically from $\mu = 0$. A single modified Gaussian peak fails to capture the starting state. The accuracy of the fits of the initial states are shown in Figures 7a and 8a for SEP(38−62)X and SEP(38−62)O, respectively. By applying the inverse mapping and the analytical expression for the starting state to eq 7, while allowing for different effective shear rates k_1, k_2, and k_3 for the subpopulations represented by the three Gaussian peaks, we obtain

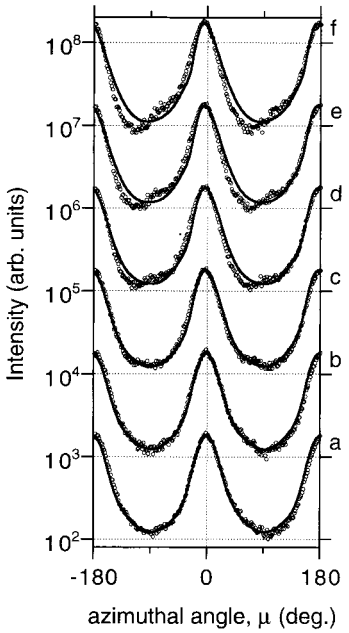

Figure 7. The solid line represents the fit of eq 10 to the steady shear data for SEP(38−62)X (data previously shown in Figure 2). No adjustable parameters are used to fit the strain dependence of the azimuthal scattering intensity, i.e., k, the effective shear rate, is taken as the applied macroscopic shear rate, 0.005 s^{-1}. The fit accurately captures the counterclockwise shift of the primary peak maximum, but predicts the behavior in the troughs up to ∼30% strain.

$$I(\mu,t) = \sum_{i=1}^{3}\frac{y_{0i} + \lambda_i \exp\{-\beta_i \sin^2[\cot^{-1}(k_i t + \cot(\mu)) - \mu_{0i}]\}}{(k_i t \sin(\mu))^2 + 2k_i t \sin(\mu)\cos(\mu) + 1} \tag{10}$$

Once the values of y_{0i}, λ_i, β_i, and μ_{0i} are adjusted to fit $I(\mu,0)$, the only parameters introduced to describe the time/strain dependence of $I(\mu,t)$ are the effective strain rates $k_1 = k_{\text{left}}$, $k_2 = k_{\text{middle}}$, and $k_3 = k_{\text{right}}$.

The solid lines in Figures 7 and 8 show the results of eq 10 when the effective shear rates are all taken to be equal to each other, thus taking eq 2 literally, and equal to the true macroscopic shear rate, giving rates $k_1 = k_2 = k_3 = 0.005$ s^{-1}. The resulting "rigid rotation model" captures the motion of the maximum in the main peak to lower (i.e., negative) values of μ, even though it is based on a microscopic model in which individual domains all rotate to higher values of μ. The reason for the counterclockwise rotation of the peak maximum will be discussed further below. This model is, however, unable to predict the observed behavior in the troughs at strains >30%, where a secondary peak develops and shifts to higher values of μ. This disparity between the data and model is more apparent in Figure 8, where the addition of silica spheres has increased the magnitude of the secondary peak.

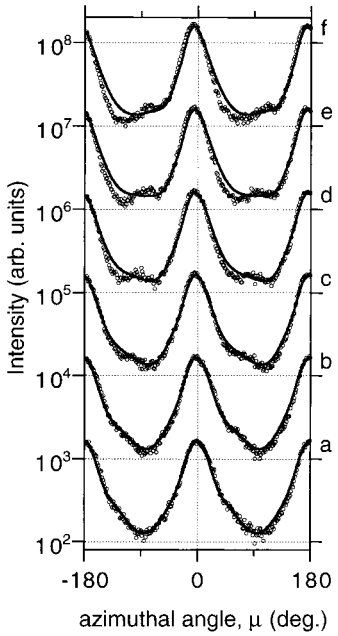

Figure 8. The solid line represents the fit of eq 10 to the steady shear data for SEP(38−62)O (data previously shown in Figure 3). Similar to Figure 7, k, the effective shear rate, is taken as the applied macroscopic shear rate, 0.005 s^{-1}. The fit accurately captures the counterclockwise shift of the primary peak maximum, but predicts the behavior in the troughs up to ∼30% strain. The failure to predict the development and shift of the secondary peak is more apparent in this sample, which contains silica spheres.

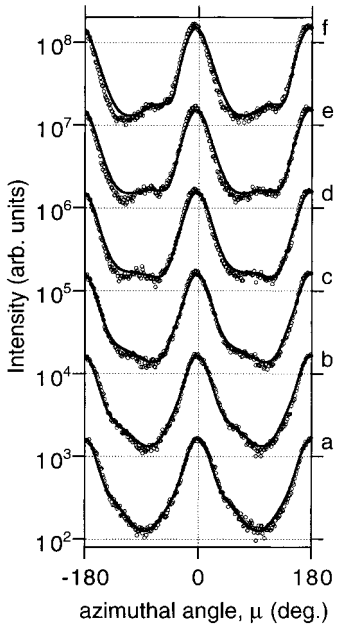

Figure 9. The solid line represents the fit of eq 10 to the steady shear data for SEP(38−62)O (data previously shown in Figure 3), with effective strain rates of $k_2 = 0.003$ s^{-1} and $k_1 = k_3 = 0.006$ s^{-1}. The fit captures both the counterclockwise shift of the primary peak maximum and the development and shift of the secondary peak.

The solid lines in Figure 9 show the application of a modified rotation model to the data for SEP(38−62)O. In this modified rotation model, the subpopulations described by the central and side Gaussian peaks have different effective shear rates: $k_2 = 0.003$ s^{-1} and $k_1 = k_3 = 0.006$ s^{-1}. The use of two effective shear rates allows us to capture both the counterclockwise shift of the maximum of the primary peak and the development and clockwise rotation of the secondary peak. Our success in describing the two salient features of the SAXS data with this somewhat ad hoc rotation model suggests that lamellar rotation (rather than boundary migration or dissolution/reformation) is the primary mechanism of both lamellar reorientation and kink band formation. However, the increase in the average rate of rotation $\dot{\mu}$ as lamellae approach the transverse orientation is more rapid than that assumed in eq 2.

The above analysis was predicated on the assumption that the total integrated scattering intensity of the fourth-order Bragg peak, integrated over both the radial and azimuthal position within the detector, is conserved during steady shear. In fact, there is a 10% and 13% loss of total intensity during the imposed 75% strain of SEP(38−62)X and SEP(38−62)O, respectively. This may be due to reorientation of lamellae out of the scattering plane or loss in coherent scattering intensity. To adjust for this loss of intensity, each of the predicted azimuthal intensity distributions, shown by the solid lines in Figures 7−9, has been normalized to the integrated intensity of the azimuthal scan to which it is compared.

Discussion

In this section we discuss initiation and growth of kink bands and the physical implications of our model regarding shear alignment of lamellar block copolymers. Microscopy studies elucidated many ideas about kink band formation in block copolymers; however, absolute determination of a mechanism requires an in situ technique, such as SAXS rheology. We will revisit two possible growth mechanisms, boundary migration and layer rotation, and on the basis of our results illustrate why a layer rotation model is more appropriate. Defect-initiated kink band formation will be discussed in the context of enhancing the secondary maximum by adding silica spheres to the diblock copolymer. Next, we will summarize the implications of our model. The significance of a lamellar rotation will be related to other observations in the area of block copolymer alignment, touching on large strain effects, strain dependence of the transverse orientation, and reversible lamellar rotation. Finally, we suggest using the distinctive changes in the azimuthal SAXS profiles, such as a counterclockwise peak shift, as an analytical tool.

Two primary models[27,28] have been proposed in the field of structural geology for kink band formation, boundary migration and layer rotation, shown schematically in Figure 10. Although these models are case-limiting scenarios, which do not consider matrix deformation and kink boundary rotation among other possibilities, they serve as useful guides to which we can compare our morphological results. Our previous electron microscopy studies revealed that kink bands produced by steady shear have strain-independent widths, a range of angles between the matrix lamellae and lamellae within the kink bands, and a lamellar dilation within the kink bands, all of which are more consistent with a layer rotation-type mechanism.[1] While electron microscopy provided evidence for this layer rotation mechanism, in situ SAXS rheology is a more appropriate experiment for studying dynamic processes. These two proposed mechanisms would correspond to different time-dependent azimuthal scattering profiles. For the boundary migration model one would expect a secondary peak to develop at an azimuthal angle corresponding to the stable orientation of lamellae within

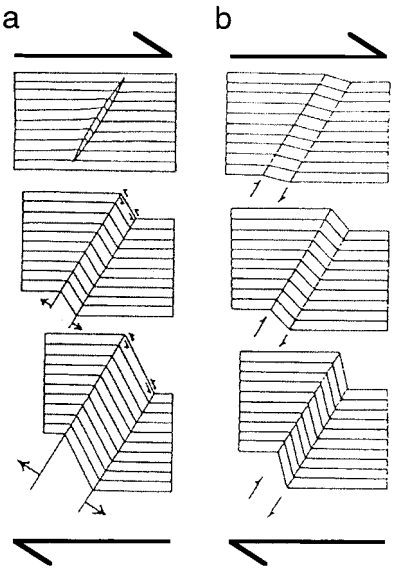

Figure 10. Schematic showing two possible mechanisms for kink band growth. The direction of shear relative to the kink bands is indicated by arrows above and below the schematics. (a) Shows a boundary migration mechanism, where a kink band initiates at a point or line defect and grows by incorporating additional material into the kink band, such that the parallel boundaries separate. In this model, the lamellar orientation is fixed inside the kink band, but the width increases with time/strain. (b) Shows a layer rotation mechanism with fixed boundaries, in which the kink bandwidth is fixed at initiation and growth occurs by a lamellar rotation between the kink band boundaries. This schematic was reproduced from ref 30.

the kink bands. This peak would grow in size, with additional strain, as the volume of kink bands increased due to widening of kink bands. However, the peak position would remain fixed. In contrast, a layer rotation mechanism should produce a peak that breaks off from the initial intensity distribution and shifts positions with strain. If the volume fraction of kinks remains constant, i.e., no increase in width, length, or depth of kink bands with strain, then this shifting secondary peak would have a constant area. Note, we are assuming that the initiation step is fast, and therefore only the growth step can be observed. However, if kink bands nucleate throughout the deformation, then the area of the secondary peaks would increase in both cases. The SAXS patterns obtained for SEP(38−62)X and SEP(38−62)O show that the shoulder of the main peak develops into a second peak and the position shifts to higher angles with strain. This observation, combined with the previous results obtained from electron microscopy, are more consistent with a layer rotation-type mechanism than a boundary migration mechanism. Furthermore, the relative area of the secondary peak does not appear to change significantly, suggesting that kink band volume does not increase at the expense of the matrix. Note that these scattering experiments are not sensitive to the orientation of the tilt (kink) boundaries, which may rotate during the deformation, contrary to the idealized model depicted in Figure 10b.

We introduced well-defined defects, 0.5-μm silica spheres, into the block copolymer in an attempt to systematically increase the volume fraction of kink bands. Electron microscopy studies previously indicated that there are two morphological requirements to form kink bands. Kink bands are observed emanating from defects and clustered around grain boundaries, which have a high defect density. Furthermore, we found that kink bands and S-folds (which appear to be precursors to kink bands) have widths that are the same characteristic size as these residual defects, ~0.5 μm. These defects produce local lamellar misorientations, which may be the instabilities that lead to kink bands. By definition, a kink band has layers that remain continuous across the kink band boundaries, which does not necessarily require that lamellae are continuous during initiation and growth. However, S-folds, observed at small strains, provide evidence that suggests that lamellar continuity is maintained during growth.[1] Therefore, a local lamellar misorientation and lamellar continuity appear to be the prerequisites for kink band formation, both of which are often observed near existing defects in an otherwise aligned morphology. Now, comparing the scattering patterns of SEP(38−62)X and SEP(38−62)O, the development of the secondary peak is enhanced in SEP(38−62)O, which contains 0.5 vol % silica spheres. This provides additional evidence that kink bands nucleate at defects in an otherwise parallel morphology and demonstrates an effective method of controlling morphology through formulation.

As the fits in Figures 7−9 illustrated, and as we will explain here, the observed counterclockwise rotation of the primary peak maximum in $I(\mu,t)$ during forward shear can be explained by a model involving purely clockwise rotation of lamellae. Equation 2 describes a rotation in which the angular velocity is always nonnegative, reaching zero for the parallel orientation and reaching a maximum for the transverse orientation. To explain the prediction by this model of a counterclockwise rotation of the peak maximum, it is useful to first consider its prediction for early times, for which the lamellae have not had time to rotate through angles approaching π, and for initial distributions in which the peaks at $\mu = 0$ and $\mu = \pi$ are narrow enough so that there is negligible intensity at the transverse orientations $\mu = \pm\pi/2$. In this limit, the fact that $I(\mu,t)$ is a periodic function becomes irrelevant, and we may discuss the evolution of $I(\mu,t)$ by considering the evolution of a single peak initially centered around $\mu = 0$ on an effectively infinite domain. Because the angular velocity vanishes at $\mu = 0$, so that lamellae can never rotate through the aligned orientation, the predicted integrated intensity of the domains $\mu < 0$ (the left half of the peak) and $\mu > 0$ (the right half of the peak) each remain constant with time. Furthermore, at early times the intensity $I(0,t)$ remains constant exactly at $\mu = 0$. The effect of the clockwise rotation is to narrow the distribution of orientations of the subpopulation with $\mu < 0$, causing a "pile up" of intensity at small negative values of μ, while broadening the orientational distribution of the subpopulation with $\mu > 0$, causing a depletion of intensity at small positive values of μ. This creates an anisotropic peak for which the position of the maximum shifts to angles $\mu < 0$. At longer times, for which the periodicity of the distribution does become relevant, the tendency of the predicted intensity to pile up at angles $\mu < 0$ is actually increased by the fact that lamellae with initial values of μ slightly greater than 0, which initially contribute to the right side of the main peak, rotate through the transverse orientation and begin to contribute to the left side of the equivalent peak at $\mu = \pi$. This is precisely what is seen in the measured scattered intensities during positive shear. Note that Okamoto et al.[6] alluded to a peak shift when they

examined a similar PS−PEP diblock using in situ SAXS rheology. They refer to a broadening, with respect to μ, of the scattered primary peak during oscillatory shear, consistent with a peak oscillating about the stable orientation. However, they collected patterns over many shear cycles, and thus the peak shift phenomenon was obscured.

The observation of a counterclockwise shift in the maximum of the main peak has important implications regarding shear-induced alignment of lamellar block copolymers. On the basis of predictions from our model regarding the evolution of the starting state distributions for SEP(38−62)X and SEP(38−62)O, the main peak shift will reverse directions at larger strains and eventually produce a δ function centered on $\mu = 0$. That is, according to this model, large strain converts a broad distribution to a narrow distribution. While these larger strains may be inaccessible because of melt fracture or other failure mechanisms, this prediction suggests that very large steady shear should be effective in aligning lamellar diblock copolymers. Studies on the effect of very large strain are currently underway in our group.

The development and shift of the secondary peak is captured by a modified rotation model, in which two effective shear rates are used for subsets of the overall population distribution. The use of a larger effective shear rate for the right and left Gaussian peaks, relative to the central peak, suggests that the mathematical form chosen for the angular velocity (eq 2) underestimates the rate of rotation of strongly misaligned material. However, the ability to capture the data with this modified differential conservation law is evidence for a rotation mechanism. A differential conservation law would, for instance, fail to describe the direct transformation of lamellae from parallel to transverse or transverse to parallel via a boundary migration or dissolution/reformation-type process. It would be useful to contrast the evolution of the 1*−2* scattering data in this study to 1*−3* scattering data for the same system prior to prealignment. One might expect that the reorientation of perpendicular lamellae (lamellar normals parallel to the 3 direction) is a two-step process: first, a transformation of the lamellar normals into the 1−2 plane, which may not obey a differential conservation law, and a lamellar rotation toward the parallel orientation, as described in this work.

A lamellar rotation mechanism also gives insight into the strain dependence of the previously observed parallel−transverse biaxial orientations. Okamoto et al.[6] and Pinheiro et al.[21] produced parallel−transverse biaxial orientations when they used 50% and 40% strain amplitude, respectively, to deform their specimens. Both groups noted that these parallel−transverse biaxial orientations remained biaxial during extensive oscillatory shear. Figures 2 and 3 show that the position of the secondary peak is located close to $\mu = 90°$ at strains in the range of 40−50% and rotates past $\mu = 90°$ at larger strains. While the position of this peak depends on the starting state, one can imagine that larger strain amplitudes would rotate all lamellae past the transverse orientation, whereas smaller strains would not be sufficient in rotating lamellae far enough. Zhang and Wiesner found that the transverse character of their biaxial orientation decreased as strain amplitude increased from 8 to 42%.[9] This may also reflect a rotation of lamellae, whereby the transverse population rotates into the parallel population to a greater extent as the strain amplitude is increased. Again, the details of the strain dependence may reflect differences in the azimuthal distributions of the starting states.

As we have shown in our previous work, steady shear applied to a predominately parallel orientation produces forward kink bands that are erased by steady shear in the opposite (negative) direction. Furthermore, steady shear in the negative direction produces a new set of forward kink bands.[1] Figure 4 shows the azimuthal intensity of SEP(38−62)O as a function of strain from 75 to 0% strain. The secondary peak follows a reverse trajectory, as compared to the positive steady shear, rejoining the main peak. This is consistent with an unwinding/erasing of forward kink bands produced during the positive steady shear. Figure 5 shows the azimuthal intensity of SEP(38−62)O as a function of strain from 0 to −75% strain. A new secondary peak develops and shifts to lower angles. This could be explained by the formation of a new set of forward kink bands relative to the negative shearing direction. This is consistent with our previous findings, illustrating that kink bands are unstable relative to reverse steady shear in a nearly parallel morphology. In contrast, oscillatory shear, applied to a nearly isotropic starting state, has trapped kink bands, producing conjugate kink bands.[22]

There has been considerable progress in mapping out domain orientation and alignment trajectories as a function of processing conditions (temperature, strain, and frequency) and molecular architecture.[2,3] However, the mechanisms responsible for these alignments have been difficult to determine. Using in situ SAXS rheology, we have clearly identified a rotation mechanism for a PS−PEP diblock copolymer in the strong segregation regime. Monitoring the main peak shift, or other subtle changes in the azimuthal intensity, may serve as an analytical tool for identifying this mechanism. In other words, one could compare the changes in the azimuthal profile to that predicted by this rotation model during steady shear in other materials or at various processing conditions. This in turn would indicate the extent to which lamellar rotation is a dominant mechanism. While a rotation mechanism may be only one of multiple mechanisms, this type of experiment would help to deconvolute the complex problem of block copolymer alignment.

We have used this technique on lower molecular weight SEP and poly(styrene-*b*-methyl methacrylate), SMMA, lamellar diblock copolymers. While the prealignments were slightly modified, the steady shear deformations were identical to those described for SEP(38−62). The lower molecular weight SEP lamellar diblock has PS and PEP blocks with weight-average molecular weights of 39 000 and 24 000, respectively, and is referred to as SEP(39−24). The prealignment process produced a peak centered on the parallel orientation, with a fwhm = 19°. Following the initial alignment, positive steady shear produced a counterclockwise shift of the peak maximum, as predicted by the rotation model, indicating that a lamellar rotation is an active alignment mechanism for this system. The SMMA lamellar diblock has PS and PMMA blocks with weight-average molecular weights of 36 000 and 29 000, respectively, and is referred to as SMMA(36−29). The prealignment process produced a very narrow distribution, fwhm = 9°, centered on the parallel orientation. In contrast to the SEP(38−62) and SEP(39−24), no peak shift was observed during steady shear. In fact, the

pattern remained practically unchanged during steady shear. Our rotation model predicts the development of a significant shoulder to the left of the main peak rather than a counterclockwise shift of the peak maximum; this difference is due to the narrow starting state distribution. The fact that no change in the azimuthal scattered intensity is observed for SMMA(36−29) illustrates that this type of experiment can differentiate the details of the alignment dynamics. Specifically, we show that keeping the nature of the styrene block constant, and changing the second block from PEP to PMMA, inhibits lamellar rotation. Additional studies are required to determine the underlying origin of this effect, e.g., if this is rooted in mechanical contrast. The manifestation of mechanical contrast in the rheology and morphological development will be examined in more detail in a future publication.[29]

Conclusions

We have demonstrated an effective approach to study oscillatory shear alignment in block copolymers: examine the effect of deformations that are fractions of an oscillatory shear cycle, deconvolute multiple effects by starting with a well-defined orientation, and enhance important morphological characteristics through formulation. This work, in conjunction with earlier microscopy studies, provides strong evidence for layer rotation-type growth of kink bands in lamellar diblock copolymers. Furthermore, we demonstrate that the volume fraction of kink bands can be controlled by systematically introducing defects, in this case 0.5-μm silica spheres. Using a rotation model we are able to predict the counterclockwise shift of the maximum in the main azimuthal scattering peak as well as the development and shift of a secondary peak. This rotation model predicts that large steady shear strain would be effective in aligning a lamellar diblock copolymer. It also provides insight into the strain dependence of the previously observed parallel−transverse biaxial orientations. More generally, we can explain the evolution of the lamellar orientation distribution during steady shear by assuming that all lamellae rotate toward the parallel orientation, as opposed to a discontinuous transformation, such as kink boundary migration or lamellar dissolution/reformation. Finally, monitoring subtle changes in the azimuthal scattered intensity can be used to confirm or reject particular alignment mechanisms as a function of the details of the material and processing conditions.

Acknowledgment. Work at the University of Pennsylvania was supported by NSF-DMR-MRSEC (9632598), NSF-DMR-YIA (9457997), and Procter & Gamble. Beam time at Daresbury Laboratory, Warrington, United Kingdom was allocated under EPSRC Grant GR/M22621. We thank the authors of the Synchrotron Radiation Source Program Library, which was used to process the SAXS data. Special thanks are to Anthony Gleeson for his valuable assistance regarding beam collimation well after standard business hours. We also thank Dr. Ian Hamley for providing the "match-stick" tools for the RSAII.

References and Notes

(1) Polis, D. L.; Winey, K. I. *Macromolecules* **1998**, *31*, 3617.
(2) Wiesner, U. *Macromol. Chem. Phys.* **1997**, *198*, 3319.
(3) Chen, Z. R.; Kornfield, J. A. *Polymer* **1998**, *39*, 4679.
(4) Winey, K. I.; Patel, S. S.; Larson, R. G.; Watanabe, H. *Macromolecules* **1993**, *26*, 2542.
(5) Winey, K. I.; Patel, S. S.; Larson, R. G.; Watanabe, H. *Macromolecules* **1993**, *26*, 4373.
(6) Okamoto, S.; Saijo, K.; Hashimoto, T. *Macromolecules* **1994**, *27*, 5547.
(7) Gupta, V. K.; Krishnamoorti, R.; Kornfield, J. A. *Macromolecules* **1995**, *28*, 4464.
(8) Patel, S. S.; Larson, R. G.; Winey, K. I.; Watanabe, H. *Macromolecules* **1995**, *28*, 4313.
(9) Zhang, Y.; Wiesner, U. *J. Chem. Phys.* **1995**, *103*, 4784.
(10) Zhang, Y.; Wiesner, U.; Spiess, H. W. *Macromolecules* **1995**, *28*, 778.
(11) Gupta, V. K.; Krishnamoorti, R.; Chen, Z.-R.; Kornfield, J. A. *Macromolecules* **1996**, *29*, 875.
(12) Gupta, V. K.; Krishnamoorti, R.; Kornfield, J. A.; Smith, S. D. *Macromolecules* **1996**, *29*, 1359.
(13) Chen, Z.-R.; Kornfield, J. A.; Smith, S. D.; Grothaus, J. T.; Satkowski, M. M. *Science* **1997**, *277*, 1248.
(14) Chen, Z.-R.; Issaian, A. M.; Kornfield, J. A.; Smith, S. D.; Grothaus, J. T.; Satkowski, M. M. *Macromolecules* **1997**, *30*, 7096.
(15) Maring, D.; Wiesner, U. *Macromolecules* **1997**, *30*, 660.
(16) Wang, H.; Kesani, P. K.; Balsara, N. P.; Hammouda, B. *Macromolecules* **1997**, *30*, 982.
(17) Kannan, R. M.; Kornfield, J. A. *Macromolecules* **1994**, *27*, 1177.
(18) Koppi, K. A.; Tirrell, M.; Bates, F. S.; Almdal, K.; Colby, R. H. *J. Phys. II France* **1992**, *2*, 1941.
(19) Koppi, K. A.; Tirrell, M.; Bates, F. S. *Phys. Rev. Lett.* **1993**, *70*, 1449.
(20) Pinheiro, B. S.; Winey, K. I. *Macromolecules* **1998**, *31*, 4447.
(21) Pinheiro, B. S.; Winey, K. I.; Hajduk, D. A.; Gruner, S. M. *Macromolecules* **1996**, *29*, 1482.
(22) Polis, D. L.; Winey, K. I. *Macromolecules* **1996**, *29*, 8180.
(23) Scott, D. B.; Waddon, A. J.; Lin, Y.-G.; Karasz, F. E.; Winter, H. H. *Macromolecules* **1992**, *25*, 4175.
(24) Spontak, R. J.; Smith, S. D.; Satkowski, M. M.; Ashraf, A.; Zielinski, J. M. In *Polymer Solutions, Blends, and Interfaces*; Noda, I., Rubingh, D. N., Eds.; Elsevier: Amsterdam, 1992; p 65.
(25) Bliss, N.; Bordas, J.; Fell, B. D.; Harris, N. W.; Helsby, W. I.; Mant, G. R.; Smith, W.; Towns-Andrews, E. *Rev. Sci. Instrum.* **1995**, *66*, 1311.
(26) Bird, R. B.; Steward, W. E.; Lightfoot, E. N. *Transport Phenomena*; Wiley: New York, 1960.
(27) Anderson, T. B. In *The Encyclopedia of Structural Geology and Plate Tectonics*; Seyfert, C. K., Ed.; Van Nostrand Reinhold Co: New York, 1987; Vol. 10, p 373.
(28) Weiss, L. E. *Tectonophysics* **1980**, *65*, 1.
(29) Polis, D. L.; Smith, S. D.; Ryan, A. J.; Winey, K. I., submitted.
(30) Ramsay, J. G. *Folding and Fracturing of Rocks*; McGraw-Hill: New York, 1967.

MA981796D